CFD and Experimental Study on Methane Hydrate Dissociation Part I. Dissociation Under Water Flow

Wu-Yang Sean
Dept. of Environmental and Ocean Engineering, University of Tokyo, 113-8656 Tokyo, Japan

Toru Sato
Dept. of Environment Systems, University of Tokyo, 277-8563 Kashiwa, Japan

Akihiro Yamasaki and Fumio Kiyono
Environmental Fluid Engineering Research Group, National Institute of Advanced Industrial Science and Technology (AIST), Tsukuba 305-8569, Japan

DOI 10.1002/aic.11060
Published online November 20, 2006 in Wiley InterScience (www.interscience.wiley.com).

Dissociation processes of methane hydrate under water flow conditions were investigated by a combination of experimental observations and numerical simulations using computational fluid dynamics (CFD). In Part I of this study, the dissociation process induced by water flow at pressures above the three-phase [hydrate (H)–liquid water (L_w)–vapor (V)] boundary in an isothermal x–P phase diagram is discussed. Dissociation experiments were carried out with a methane hydrate ball (diameter $\cong$ 10 mm) suspended in a flow cell, and the overall dissociation rate of methane hydrate without bubble formation was measured under various conditions of pressure, temperature, and volumetric flow rate of water. A linear phenomenological rate equation in the form of the product of the dissociation rate constant k_{bl} and the molar Gibbs free energy difference ΔG, between the hydrate phase and the ambient aqueous phase, was derived by considering the Gibbs free energy difference as the driving force for the dissociation. The molar Gibbs free energy difference was expressed by the logarithm of the ratio of the concentration of methane dissolved in water at the hydrate surface to the solubility of methane in the aqueous solution in equilibrium with the hydrate. The dissociation rate constant k_{bl} was determined from the experimental results of the overall dissociation rate combined with the numerical simulation results of the concentration profile of methane by the CFD method. The obtained dissociation rate constant was found to be independent of the ambient water flow rate, indicating that the rate constant is intrinsic for the hydrate dissociation within the conditions examined in this study. The rate constant was independent of the pressure, whereas the temperature dependency was described by an Arrhenius-type equation with the apparent activation energy of 98.3 kJ/mol. © 2006 American Institute of Chemical Engineers *AIChE J,* 53: 262–274, 2007

Keywords: methane hydrate, dissociation rate constant, hydrate dissociation model, CFD, mass and heat transfer

Correspondence concerning this article should be addressed to A. Yamasaki at aki-yamasaki@aist.go.jp.
W.-Y. Sean is currently at Asia-Pacific Business Division, International Business Center, Industrial Technology Research Institute, TTD Bldg. 3F, 1-2-18, Mita, Minato-ku, Tokyo 108-0073, Japan.

Introduction

Methane hydrate (MH) buried in deep marine sediments has been recognized as a potential future energy resource because an enormous amount of methane is estimated to be trapped in methane hydrate sediments. Methane hydrate is a clathrate compound, in which a cage-like lattice structure formed by hydrogen-bonded water molecules can trap methane molecules and be stabilized. Methane hydrate is more stable under lower temperature and higher pressure conditions. It is necessary to dissociate methane hydrate to produce methane gas from the methane hydrate layer in marine sediments. Several methods have been proposed to recover methane gas from the methane hydrate layer; including depressurization, warm water supply, and injection of an inhibitor to promote dissociation of the hydrate. An accurate method for estimating the dissociation rate of methane hydrate would be necessary to predict the gas production rate from a given methane hydrate–bearing layer.

The apparent dissociation rate of methane hydrate may reflect various transport processes such as heat and mass transfer, in addition to the intrinsic dissociation reaction of methane hydrate itself. In most of the previously proposed models for the dissociation of hydrates, the heat transfer process is assumed to be the rate-determining step because a large amount of dissociation heat needs to be supplied to advance the hydrate dissociation process. In such cases, the dissociation process of hydrate is equivalent to the heat transfer process, which could be represented by the rate at which the dissociation temperature for the hydrate progresses.[1–5]

However, the apparent dissociation rate would, in general, include the mass transfer rate and the intrinsic dissociation rate at the hydrate surface as well as the heat transfer rate. It is necessary to evaluate all the rates of mass transfer, heat transfer, and the intrinsic dissociation for an accurate prediction of the apparent hydrate dissociation rate. When a sufficient amount of heat for dissociation can be supplied from the ambient, the heat transfer process would not necessarily be the rate-determining step of the hydrate dissociation. An example is the hydrate dissociation process under a water flow, of which the flow rate is sufficiently high to supply an adequate amount of heat for dissociation. Another example can be found for the initial stage of the methane hydrate dissociation in a sediment layer by depressurization, where the heat of dissociation could be supplied from the ambient sediment until the temperature reaches the equilibrium temperature for a given pressure. For such cases, the dissociation rate should be expressed by the combination or balance of the mass transfer and the intrinsic dissociation rate. Therefore, information of the intrinsic dissociation rate is important or even essential for the prediction of production rates of natural (methane) gas from the methane hydrate sediments.

Bishnoi and coworkers emphasized the importance of the intrinsic rate of the hydrate dissociation. A series of experiments were conducted in stirred tank-type reactors by their group. To measure the intrinsic dissociation rates of hydrates, the effects of mass and heat transfer resistances were eliminated by vigorous stirring in the reactor. Based on the experimental results, Kim et al.[6] proposed a rate equation (Kim–Bishnoi equation) for the intrinsic dissociation rates based on the fugacity difference between the point at which dissociation takes place and the equilibrium condition, and the rate constants have been determined. More accurate measurements were performed by Clarke and Bishnoi[7] with a particle-size analyzer. The Kim–Bishnoi equation has been used for a variety of dissociation processes, including a simulation of methane production from marine hydrate sediment. However, elimination of the heat transfer and mass transfer resistances was carried out simply by increasing the stirring rate in batch-type reactors in their treatments. Although a rate constant above a certain stirring rate was observed, further work is required to confirm elimination of the heat and mass transfer resistances because such resistances can sometimes become saturated at increased stirring rates. In such cases, it is impossible to eliminate the heat or mass transfer resistances from the apparent dissociation rate to obtain the intrinsic dissociation rate.

The primary objective of the present study was to develop a new method to determine the intrinsic dissociation rate constant of methane hydrate by a combination of experimental observations and numerical simulations with a computational fluid dynamics (CFD) method. In this study, dissociation processes of methane hydrate under fresh water flow were investigated. The advantage of the present method is that the intrinsic dissociation rate can be evaluated separately from the mass transfer rate, which enables us to investigate the dissociation processes at a wider range of water flow rates. In Part I of this study, the dissociation process of methane hydrate at pressures above the three-phase [hydrate (H)–liquid water (L_w)–vapor (V)] boundary line will be discussed. Under such conditions, methane hydrate dissociation would be driven only by the pure water flow. The dissociation rate equation was derived for the dissociation process on the basis of the molar Gibbs free energy difference and the dissociation rate constant was determined under various conditions of water flow rate, pressure, and temperature. The obtained rate constant was found to be independent of the flow rate, to ensure that it is intrinsic at least under the present conditions. In Part II, the determined values of the dissociation rate constant will be applied to the dissociation process driven by depressurization, to examine the universality of the dissociation rate equation and the rate constant that are based on the molar Gibbs free energy difference as the driving force. An early study of the present work was presented by Sean et al.[8]

Theoretical Treatment: A Dissociation Model Formulation of the Dissociation Rate Equation

A schematic phase diagram of the mole fraction of methane (x) and the pressure (P) for the water–methane–hydrate system at a constant temperature is shown in Figure 1. Consider a two-phase [L_w (liquid water)–H (hydrate)] coexistence system, where the hydrate phase (denoted by point N) is equilibrated with the water phase saturated with methane (denoted by point M). The equilibrium solubility of methane in the aqueous phase (at point M) is given by x_{eq} (in mole fraction).

Suppose the methane concentration in the water at the surface of the hydrate is reduced to $x_I (x_I < x_{eq})$, which is below the equilibrium solubility x_{eq}, with keeping the pressure and

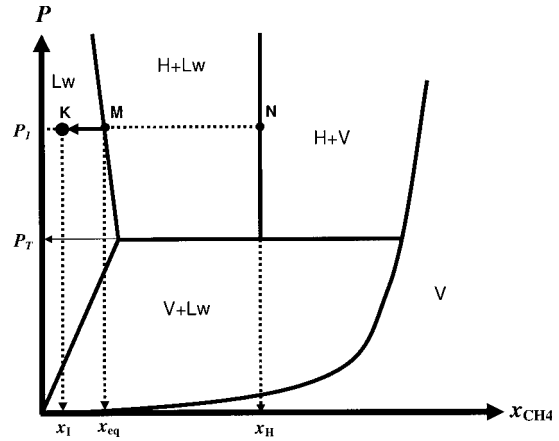

Figure 1. Schematic drawing of the mole fraction–pressure (*x–p*) phase diagram for methane–water–hydrate (temperature constant).

temperature conditions constant. Such a state can be denoted by point K in Figure 1. The hydrate would dissociate because only the aqueous phase (L_w) is stable under such conditions. To formulate such a dissociation process from a two-phase (H–L_w) coexisting condition to a single aqueous phase (L_w) condition, the following assumptions were made.

Driving force for the dissociation

Kashchiev and Firoozabadi[9] formulated the hydrate formation process by using the molar Gibbs free energy of the guest gas and water. This study is based on the same concept: we assume the driving force for the dissociation is expressed by the change of the Gibbs free energy when one mole of the hydrate (consisting of one mole of methane and h_w moles of water, where h_w is the hydration number) is dissociated into the ambient aqueous solution. The free energy of the hydrate phase G^H, per one mole of hydrate, can be expressed by:

• Hydrate phase

$$G^H = \mu_M^H + h_w \mu_W^H \tag{1}$$

where μ_M^H and μ_W^H are chemical potentials of methane and that of water in the hydrate, respectively. When one mole of the hydrate is dissociated to an aqueous solution, the free energy after dissociation is given by

• Ambient aqueous phase

$$G^L = \mu_M^L + h_w \mu_W^L \tag{2}$$

where μ_M^L and μ_W^L are chemical potentials of methane and that of water, respectively, in the ambient aqueous solution. Thus, the driving force for the dissociation ΔG is given by

$$\Delta G = G^H - G^L = (\mu_M^H - \mu_M^L) + h_w(\mu_W^H - \mu_W^L) \tag{3}$$

Dissociation rate formulation

In this study, it is assumed that the dissociation flux (F_1) is proportional to the driving force, the free energy difference ΔG, expressed as

$$F_1 = k_{bl} \Delta G \tag{4}$$

where k_{bl} is the rate constant. In this study, it is assumed that the dissociation rate is expressed by Eq. 4. Such a linear phenomenological equation can be rationalized according to the thermodynamics of irreversible processes.[10] However, the validity of the Eq. 4 can be verified by checking whether the determined kinetic coefficient in Eq. 4, k_{bl}, is constant for given temperature and pressure conditions, irrespective of the ambient water flow or concentration conditions.

Formulation of the free energy difference in terms of the solubility

The molar Gibbs free energy terms in Eq. 3 were expressed in terms of the chemical potential of each component in the phases. The chemical potential terms can be converted into the solubility terms of methane in the aqueous phase, which are directly measurable properties.

• The hydrate phase

The hydrate (denoted by point N in Figure 1) is equilibrated with the aqueous solution (point M) of which the concentration of methane is equal to the equilibrium solubility x_{eq}. The chemical potential of methane in the hydrate phase equals that in the aqueous phase in which the methane concentration is x_{eq} under the same temperature and pressure conditions, and the same for water as well. The chemical potentials of methane and water in the aqueous solution μ_M^L and μ_W^L can be expressed by the following equations as a function of the mole fraction of methane x_{eq}:

For Methane

$$\mu_M^L(M) = \mu_M^* + RT \ln \gamma_M x_{eq} \qquad \text{(aqueous phase)} \tag{5}$$

For Water

$$\mu_W^L(M) = \mu_W^0 + RT \ln \gamma_W (1 - x_{eq}) \qquad \text{(aqueous phase)} \tag{6}$$

where μ_M^* and μ_W^0 are the chemical potentials of the reference states, respectively of methane and water. γ_M and γ_W are activity coefficients of methane and water, respectively. According to the asymmetric convention, the reference state of the chemical potential for water is set as pure water ($x_{eq} = 0$) and that for methane dissolved in water is set as the state extrapolated to $x_{eq} \to 0$, where the activity coefficient is unity.[11] Because of the extremely low solubility of methane in water, the activity coefficients of both water and methane can be approximated as unity for the conditions studied. Then the equilibrium conditions between the hydrate phase and the aqueous phase can be given by:

For Methane

$$\mu_M^H(N) = \mu_M^L(M) = \mu_W^* + RT \ln x_{eq} \tag{7}$$

For Water

$$\mu_W^H(N) = \mu_W^L(M) = \mu_M^0 + RT \ln(1 - x_{eq}) \tag{8}$$

• The ambient aqueous phase

The chemical potentials of water and methane in the ambient aqueous solution at the surface of the hydrate can be

expressed by equations similar to Eqs. 5 and 6, substituting the equilibrium mole fraction of methane (x_{eq}) by the nonequilibrium mole fraction of methane at the point by K in Figure 1 (x_I).

For Methane

$$\mu_M^L(K) = \mu_M^* + RT \ln x_I \tag{9}$$

For Water

$$\mu_W^L(K) = \mu_W^0 + RT \ln(1 - x_I) \tag{10}$$

where μ_{M}^* and $\mu_{\mathrm{M}}^0$are the chemical potentials of the same reference states as those in Eqs. 7 and 8, respectively. Therefore, the free energy difference ΔG, between the states of the hydrate phase (N) and the ambient water phase (K), can be given by

$$\Delta G = G^H(\mathrm{N}) - G^L(\mathrm{K}) = G^L(\mathrm{M}) - G^L(\mathrm{K}) = RT \ln \frac{x_{eq}}{x_I} + h_w RT \ln \frac{1 - x_{eq}}{1 - x_I} \tag{11}$$

Because the mole fractions of methane in the aqueous phase (x_{eq}, x_I) are extremely low (in the order of about 10^{-6}–10^{-7}), and the hydration number is about 5–6, the second term in the right-hand side of Eq. 11 can be neglected in comparison to the first term. Then ΔG can be approximated by

$$\Delta G = RT \ln \frac{x_{eq}}{x_I} \tag{12}$$

Note Eq. 12 could be derived directly by considering only the chemical potential difference of methane between the hydrate phase and the aqueous phase, $\mu_M^H(\mathrm{N}) - \mu_M^L(\mathrm{K})$ or, equivalently, the chemical potential difference of methane between the equilibrium and ambient aqueous phases, $\mu_M^L(\mathrm{M}) - \mu_M^L(\mathrm{K})$. By inserting Eq. 12 into Eq. 4, the rate equation can be rewritten as

$$F_1 = k_{bl} RT \ln \frac{x_{eq}}{x_I} \tag{13}$$

Thus, the dissociation equation can be simply expressed by the product of the proportionality constant k_{bl} and the logarithm of the ratio of mole fraction of methane in the aqueous solution at equilibrium with hydrate x_{eq}, to that in the ambient aqueous solution at the surface of the hydrate x_I. The ratio of the mole fractions can be replaced by the ratio of the volumetric molar concentrations because of the extremely low mole fraction of methane dissolved in water, that is,

$$F_1 = k_{bl} RT \ln \frac{C_H}{C_I} \tag{14}$$

where C_H and C_I are the volumetric molar concentrations of methane (mol/m^3) in the aqueous phase equilibrated with hydrate and in the ambient aqueous phase at the hydrate surface, respectively.

Method of determination of the intrinsic dissociation rate constant k_{bl}

The experimentally observable dissociation rate (overall dissociation rate, hereafter denoted by F_{obs}) would be the sum of the local dissociation rates, depending on the local surface concentration C_I, which is unknown. Because the measurement of F_{obs} in water flow is not sufficient to obtain the two unknowns—k_{bl} and C_I—a CFD technique with local mass and heat transfer was adopted in this study. The following method was used to determine the dissociation rate constant k_{bl} from the experimental result for the overall dissociation rate in combination with the CFD technique.

1. Measurement of the Overall Dissociation Rate from a Hydrate Ball. A dissociation experiment was conducted from a methane hydrate ball located in a flow of water with a known volumetric flow rate Q, under given conditions of temperature T and pressure P. The overall dissociation rate F_{obs} can be determined from the average concentration of dissolved methane C_x, which was measured at a distant location downstream from the hydrate, where the methane concentration is uniform over the cross section of the flow. The overall dissociation rate is given by

$$F_{obs} = QC_x \tag{15}$$

2. Preparation of a Calibration Curve for k_{bl} from C_x. First a certain value of the dissociation constant k_{bl} was assumed. Then, the profile of the flow velocity and the concentration of methane in the ambient water around the hydrate were simulated by the CFD method with the assumed value of k_{bl}. The boundary condition for the methane concentration at the surface of the hydrate can be given by

$$k_{bl} RT \ln \frac{C_H}{C_I} = D\nabla C \tag{16}$$

where D and C are, respectively, the diffusion coefficient and the concentration of methane in the aqueous phase in the vicinity of the surface. C_I is unknown and calculated by Eq. 16 locally at each surface cell. Literature data are available for the solubility of methane in water equilibrated with hydrate C_H.[12] From the surface concentration profile, the overall dissociation rate or, equivalently, the average concentration of methane can be numerically calculated against the assumed value of the dissociation constant k_{bl}. Practically, a calibration curve between k_{bl} and C_x was drawn by varying the dissociation rate constant k_{bl}, which can be determined as the value on the calibration curve corresponding to the experimentally observed value of C_x.

Computational Fluid Dynamics Method

Basic transport equations and boundary conditions

The following are the basic equations and assumptions for the fluid dynamic model.

It is assumed that ambient fluid is incompressible and no bubble formation occurs in the flow. The continuity and the Navier–Stokes equations for the aqueous phase are given by

$$\nabla \cdot \boldsymbol{u} = 0 \tag{17}$$

$$\frac{\partial u}{\partial t} + \boldsymbol{u} \cdot \nabla \boldsymbol{u} = -\frac{1}{\rho} \nabla p + v \nabla \cdot [\nabla \boldsymbol{u} + (\nabla \boldsymbol{u})^T] \tag{18}$$

where $\boldsymbol{u}$ is the flow velocity, p is the fluid-mechanical static pressure, ρ is the water density, and v is the kinematic viscosity of water.

Mass transfer of dissolved methane in the ambient flow can be described by the advection–diffusion equation:

$$\frac{\partial C}{\partial t} + \boldsymbol{u} \cdot \nabla C = D\nabla^2 C \tag{19}$$

where D is the diffusion coefficient of methane in water.

Heat transfer in the ambient flow is caused by convection and the conduction in the flow is assumed to be negligible. Heat transfer inside the hydrate ball is caused by conduction. The heat transfer process can be given by the following equations:

$$\frac{\partial T}{\partial t} + \boldsymbol{u} \cdot \nabla T = \alpha_L \nabla^2 T \qquad \text{(in the aqueous phase)} \tag{20}$$

$$\frac{\partial T}{\partial t} = \alpha_H \nabla^2 T \qquad \text{(in the hydrate phase)} \tag{21}$$

where T is the temperature and α_L and α_H are the heat diffusivities in the aqueous and hydrate phases, respectively.

Boundary conditions for the mass transfer of methane and for the heat transfer are given by combining the dissociation equation (Eq. 14) of the hydrate ball with the transport flux at the surface of the hydrate ball. Thus, the boundary conditions are given as

$$k_{bl} RT \ln \frac{C_H}{C_I} = D\nabla C \qquad \text{(mass transfer of methane)} \tag{22}$$

and

$$q_H + \lambda_H \nabla T_H = \lambda_L \nabla T_L \qquad \text{(heat transfer)} \tag{23}$$

where q_H ($= \Delta H_{dis} \times F_1$, where ΔH_{dis} is the latent heat of hydrate dissociation) is the rate at which the latent heat is transferred to the methane hydrate by dissociation; λ_H and λ_L are the heat conductivities in the hydrate and water, respectively.

Physical properties for the CFD calculation

The following physical properties are used for the CFD calculations:

- Heat of dissociation

Heat of dissociation per mole hydrate ΔH_{dis} is given by Kuustraa and Hammershaimb[13] as

$$\Delta H_{dis} = 56,599 - 16.744 T_I \ (J \text{ mol}^{-1}) \tag{24}$$

where T_I is the surface temperature.

- Physical properties of the aqueous phase

The following empirical functions of the temperature were cited from a handbook:[14]

Kinematic Viscosity

$$v_L = (8.8286 \times 10^{-10})T^2 - (5.3886 \times 10^{-7})T + 8.3104 \times 10^{-5} \ (\text{m s}^{-2}) \tag{25}$$

Diffusion Coefficient of Methane in the Aqueous Phase

$$D = (1.2398 \times 10^{-12})T^2 - (6.7677 \times 10^{-10})T + 9.4190 \times 10^{-8} \ (\text{m s}^{-2}) \tag{26}$$

Heat Conductivity

$$\lambda_L = 487.85 \ln T - 2173.8 \ (\text{W K}^{-1} \text{ m}^{-1}) \tag{27}$$

- Physical properties of solid hydrate

The following literature data were used for the physical properties of the methane hydrate:[15]

Thermal Diffusivity in the Aqueous Phase

$$\alpha_L = 9.78 \times 10^{-8} \text{ m s}^{-2}$$

Heat Capacity of the Hydrate at Constant Pressure

$$C_{pH} = 2010 \text{ J kg}^{-1} \text{ K}$$

Heat Conductivity in the Hydrate Phase

$$\lambda_H = 0.393 \text{ W K}^{-1} \text{ m}^{-1}$$

The value of $\rho_H = 910$ kg/m^3 measured in the present study was used for the density of the methane hydrate ball.

- Solubility of methane in the water

The following correlation equation was derived for the solubility of methane equilibrated with hydrate x_{eq}, based on the experimentally measured results by Seo and Ryu:[12]

$$x_{eq} = 1.0 \times 10^{-3} \times [-0.01P + (2.23 \times 10^{-4}) \exp(0.0319T)] \tag{28}$$

The numerical simulation method

Computational Domain and Grid System. We used a three-dimensional unsteady CFD code developed by Jung and Sato[16] that adopts collocated finite-volume formulation and moving unstructured grids. This method has successfully been used to predict the behavior of a rising and deforming droplet. The methane hydrate ball can be regarded as a solid and thus grids around the ball were fixed in this study. For the inflow and the outflow boundaries, a laminar parabolic velocity profile and the zero-gradient Neumann condition were imposed, respectively. A no-slip condition was used on the sidewall and the surface of the methane hydrate ball.

The computational domain was in conformity with the cylindrical observation cell of the experimental facility. Upward and downward were the inflow and outflow boundaries, respectively, although they were opposite in the experimental configuration, as is described later. The vertical flow direction, however, has no effect on the simulation because the gravity effect was excluded in Eq. 18, considering the boundary condition for hydrostatic pressure. The methane hydrate ball was set on the axis of the cylindrical domain at a distance of 20 mm from the inflow, whereas the ball was positioned at a distance of 80 mm from the inflow in the experiment. This is also not a problem because a velocity boundary condition at the inflow, a fully developed laminar cylindrical Poiseuille flow, which is expected at 80 mm downflow of the real inlet, was imposed. The inside of the flow cell was discretized into unstructured grids, as shown in Figure 2. There were two types of computational cells—tetrahedrons and triangular prisms—the latter of which were arranged on the methane hydrate surface and the former were applied to the other spaces including the inside of the

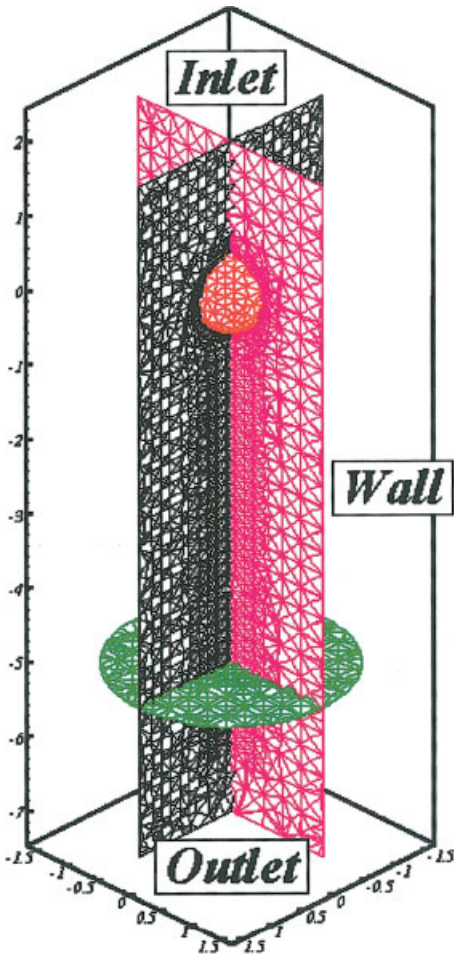

Figure 2. Schematic image of computational cells near MH surface for the mass transfer.

[Color figure can be viewed in the online issue, which is available at www.interscience.wiley.com.]

methane hydrate ball, for heat transfer. The grids in the wake of the ball were concentrated on to resolve shed vortices. We adopted the special feature of the method of Jung and Sato,[16] that is, one cell layer of the prisms, attaching to the methane hydrate surface, was divided into very thin layers (VTLs) of prisms to resolve thin mass and heat boundary layers, as is shown schematically in Figure 3. The numbers of prism layers and VTLs were set at 15 and 10, respectively. For resolving boundary layers by these grids, the thickness of each grid should be sufficiently smaller than the boundary layer thickness. The thicknesses of the boundary layers for momentum transport δ_m and for the mass transport δ_c were given by Jung and Sato:[16]

$$\delta_c = \frac{\delta_m}{1.026\mathrm{Sc}^{1/3}} \tag{29}$$

$$\delta_m = \frac{5.48}{\sqrt{\mathrm{Re}}}\frac{d}{2} \tag{30}$$

where Re and Sc are the Reynolds and the Schmidt numbers, respectively. The minimum thicknesses of the boundary layers for mass transfer are listed in Table 1, and these correspond to the maximum Reynolds and Schmidt numbers (Re = 252 and Sc = 1965) for the present experimental systems. It was confirmed that the thickness of the present grids (Δ) was sufficiently smaller than the minimum boundary layer thicknesses to resolve the corresponding boundary layers. The VTL size for temperature was set at the same value, assuming that the mass boundary layer is in general thinner than that of heat transfer.

The boundary condition at the surface of the hydrate in Eq. 22 can be expressed in a discrete form

$$k_{bl}RT\ \frac{C_H}{C_I} = D\frac{C_I - C'}{h_L} \tag{31}$$

where C' is the methane concentration at the centroid of a cell attaching to the methane hydrate surface and h_L is the length of the water layer attached to the hydrate surface, as shown in Figure 4.

The boundary condition for the heat transfer in Eq. 23 can be converted to the surface temperature T_I, in combination with the latent heat necessary for the phase change in Eq. 24 by

$$T_I = \frac{\lambda_L h_H T_L + \lambda_H h_L T_H - 56,599\ F_1 h_L h_H}{\lambda_L h_H + \lambda_H h_L - 16.744\ F_1 h_L h_H} \tag{32}$$

where T_L and T_H are the temperatures defined at the centroids of a cell in the aqueous phase and at a cell in the solid hydrate, respectively; these cells are attached to the hydrate surface, as shown in Figure 5.

Computational Schemes. For the convection–diffusion equations for momentum, mass, and temperature, a third-order upwinding scheme and a second-order central differencing scheme were adopted to approximate the convection and the diffusion terms, respectively. The time differential terms were discretized by a second-order explicit scheme. Pressure and velocity were coupled based on the marker and cell (MAC)–type fractional step method. Incompressible flux at each cell face, originally introduced in Rhie and Chow,[17] was taken into account in the pressure calculation for the numerical stability of the present collocated-grid method.

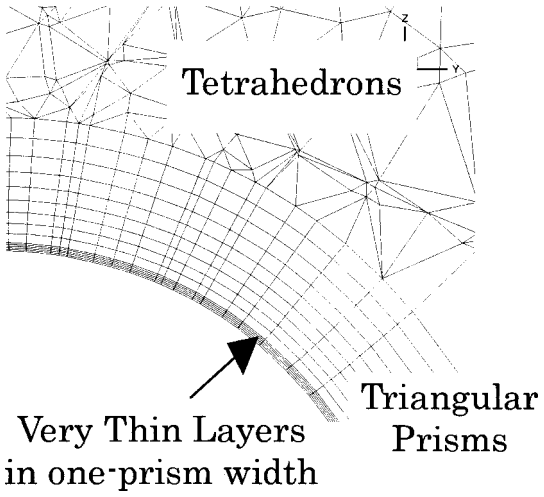

Figure 3. Grid arrangements for CFD near the MH surface.

Table 1. Thicknesses of the Boundary Layers δ and Computational Grid Δ, at Re = 252 and Sc = 1965

Total Number of Grids	Number of Surface Grids	$\delta_m(m)$, $\times 10^{-3}$	$\Delta_m(m)$, $\times 10^{-3}$	$\delta_c(m)$, $\times 10^{-4}$	$\Delta_c(m)$, $\times 10^{-4}$
74,379	1544	1.73	0.10	1.34	0.10
48,413	379		0.10		0.10

Validation of the CFD Code. The CFD code was examined by comparing the calculated results for Sherwood number (Sh) and drag coefficient (C_d) with those obtained by empirical correlations. For the comparison of dissolution, we picked up three empirical correlation equations of Sh for a sphere in a flow: Rowe and Claxton,[18] Whitaker,[19] and Ranz and Marshall,[20] the valid ranges of which are $20 < Re < 2000$ and $1200 < Sc < 2770$; $3.5 < Re < 76{,}000$ and $Sc < 380$; and $20 < Re < 70{,}000$ and $Sc < 400$, respectively. Therefore, only the Rowe–Claxton equation covered both Re and Sc for the present experiment conditions. The Sh difference between the CFD and the Rowe–Claxton is 7.2%, which is considered as one of the errors when calculating the rate constant, as is shown later. In these simulations for validation, C_I was set constant. For the drag coefficient C_d, empirical correlation equations by Lapple[21] and Clift et al.[22] were used for comparison. As shown in Tables 2 and 3, the calculated values for C_d and Sh were in good agreement with the values obtained by the empirical correlations under the same conditions. Therefore, it was confirmed that the present code can be applied to the present system.

Experimental System and Procedure for the Dissociation Flux Measurements

Experimental apparatus

Figure 6 shows a schematic drawing of the experimental apparatus for the methane hydrate dissociation. The apparatus, a water flow system operated under high-pressure conditions, is composed of an observation section, where a methane hydrate ball is placed for dissociation and a high-pressure pump for the water flow. The main part of the observation section was constructed from two coaxial cylindrical tubes of Pyrex® (outer) and polycarbonate (inner). Between the outer and inner tubes, temperature-controlled water was circulated to maintain the experimental temperature. The inner diameter of the polycarbonate tube was 30 mm and the length was 100 mm. The maximum bearing pressure for the polycarbonate tube was about 10 MPa. Each end of the polycarbonate tube was connected to a tapered tube of polycarbonate with a stainless steel flange. The inner diameter of the tapered tube was 30 mm at one end and 10 mm at the other end, and the length was 100 mm. The rest of the flow system was made from stainless steel tubing with an inner diameter of 10 mm. Precooled water was supplied to the system with a hydraulic pump with three cylinders to avoid flow fluctuations. The flow rate was controlled over a range up to 2.0 L/min and was monitored by a turbine-type flow indicator. The pressure was controlled by a back-pressure–regulating valve installed at the downstream side of the flow system and the pressure was monitored by a high-pressure sensor.

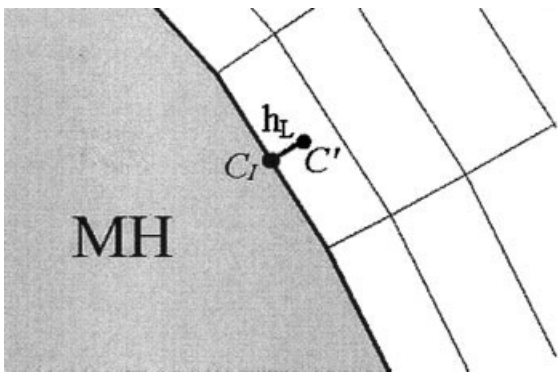

Figure 4. Schematic image of computational cells near the MH surface for the mass diffusion.

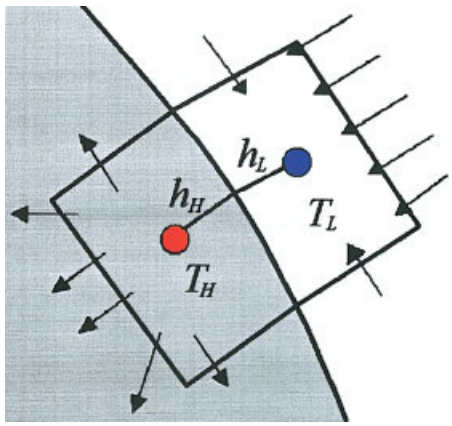

Figure 5. Schematic image of computational cells near the MH surface for heat transfer.

[Color figure can be viewed in the online issue, which is available at www.interscience.wiley.com.]

Preparation of methane hydrate balls

Fine methane hydrate powder was prepared from fine ice powder by the ice–gas interface method.[23,24] The fine ice powder was prepared by condensation of atmospheric water vapor onto a plate cooled by liquid nitrogen. The ice powder was then converted into hydrate powder in a high-pressure vessel under high pressure with pure methane gas (about 8.5–10 MPa) at a temperature near the melting point of ice (271–275 K). The ice powder was converted almost completely into methane hydrate powder after several days of mixing. A given amount of the hydrate powder was then mounted in a pair of half-spherical molds made of stainless steel, the inner diameters of which were 0.01 m. Both

Table 2. Calculated Sherwood Number Sh, at Re = 155 and Sc = 1965

	Sh			
Total Number of Grids	CFD	Rowe–Claxton	Whitaker	Ranz–Marshall
74,379	113	125	140	95
48,413	116			

Table 3. Calcualted Drag Coefficient C_d, at Re = 155 and T = 276.15 K

Total Number of Grids	C_d		
	CFD	Clift	Lapple
74,379	0.88	0.89	0.87
48,413	0.89		

molds had a groove on the edge for an iron skewer of diameter 0.1 mm. The pair of the half-spherical molds were then joined together with an iron skewer being placed between the modules, and the sphere was pressurized by an oil jack at a pressure of 8.0 MPa. Finally, a spherical ball of methane hydrate 1 cm in diameter, skewered on the iron wire, was obtained.

Dissociation experiments

The hydrate ball was mounted in the observation tube, hooked to the flange with the iron wire. The center of the ball was located 2 cm below the upper end of the cylindrical observation tube. Precooled pure water was supplied to the system by the high-pressure pump at a given flow rate. The pressure was increased to a specified value by adjusting the back-pressure–regulating valve. The water flow was one-way; fresh water was fed into the system during the experiment. The dissociation process was observed directly through the observation tube. Concentration of the dissolved methane in water was determined by analyzing the composition of the aqueous phase by gas chromatography (GC). Sampling of the liquid was conducted at a location about 50 cm downstream from the observation tube. The water in the main flow line was introduced into the sampling line through a high-pressure valve. The sampling line was made from a stainless steel pipe with 2 m length and 1/32-in. outer diameter. The pressure drop in the line was sufficiently large to keep the pressure in the main flow and to reduce the downstream pressure to atmospheric pressure. The sampled liquid was vaporized in the sampling line and the vapor was introduced to a GC to analyze the water content and the methane content detected by a thermal conductivity detector (TCD) and flame ionization detector (FID), respectively. The sampling was performed 10 min after the pure water flow was started. The dissociation experiments were conducted at pressures above the three-phase (H–L_w–V) boundary pressure for a given temperature. Temperature was varied over the range of 276.15–283.15 K.

Results and Discussion

Numerical simulations of the methane hydrate dissociation

Typical results for the numerical simulation of the methane hydrate dissociation, velocity vectors, and contour maps for the temperature and concentration of dissolved methane in water are shown in Figure 7. The parameters were set to $k_{bl} = 2.0 \times 10^{-6}$ mol^2 J^{-1} s^{-1} m^{-2}, $Q = 1.36 \times 10^{-5}$ m^3 s^{-1}, $P = 7.0$ MPa, and $T = 280.15$ K. The elapsed time after the start of dissociation was 46.92 s and the initial temperature of the methane hydrate ball was set to 253.15 K. Formation of a laminar ring-type vortex in the wake was observed as shown in Figure 7a, corresponding to the relatively low Reynolds number, Re = 135. Figure 7b demonstrates that the concentration of methane at the surface of the methane hydrate ball (C_I) was not uniform during the dissociation under flow conditions. The result indicates that a local difference in mass concentration can be observed. Figure 7c shows

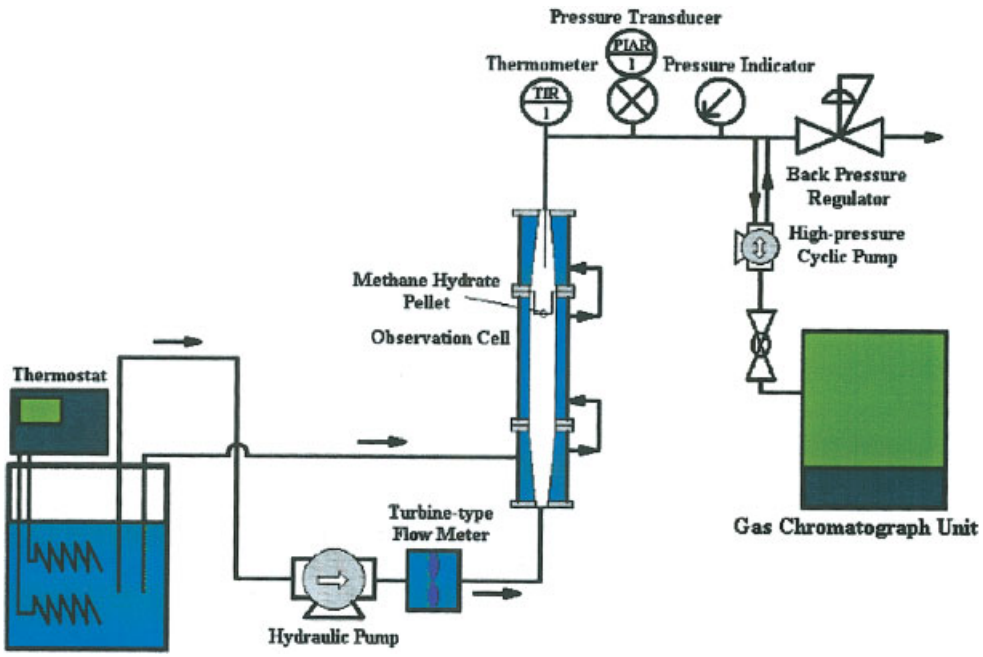

Figure 6. Schematic drawing of the experimental apparatus for the methane hydrate ball dissociation study.

[Color figure can be viewed in the online issue, which is available at www.interscience.wiley.com.]

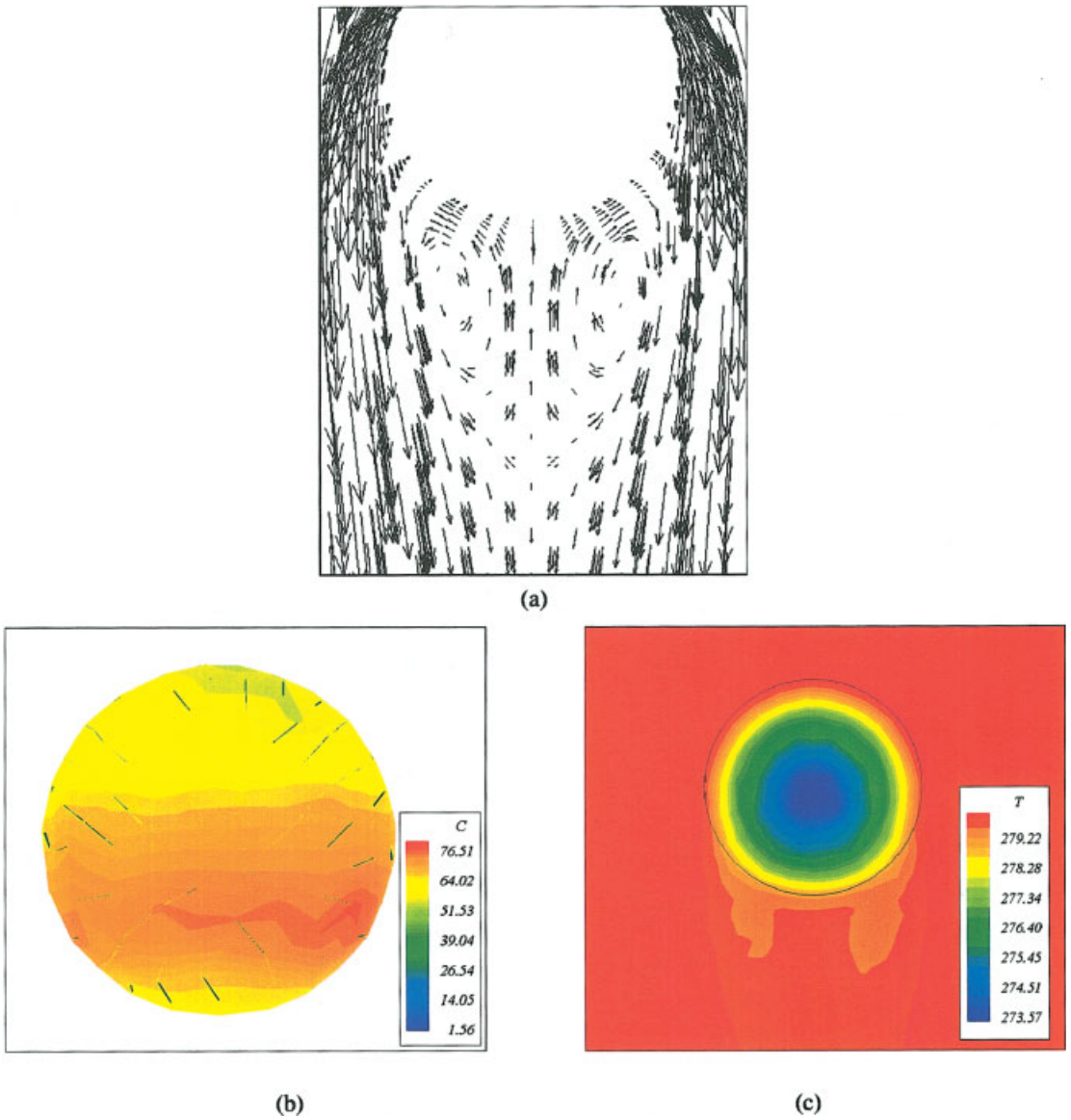

Figure 7. Velocity vectors and contour maps of temperature in the vicinity of the MH ball and of mass concentration on the pellet 46.92 s after the start of flow at $Q = 1.36 \times 10^{-5}$ m^3 s^{-1}, $P = 7.0$ MPa, and $T = 280.15$ K.

The initial temperature of the methane hydrate ball was 253.15 K.

the temperature profile for the system. Although the temperature profile inside the methane hydrate was nonuniform, the temperature in the vicinity of the surface of the methane hydrate was almost constant and equal to that of the ambient water flow, which was almost constant. Thus, the heat transfer resistance between the surface of the methane hydrate and the ambient water was negligibly low and, consequently, the surface temperature could be assumed to be equal to the water temperature. Thus, it was confirmed that the dissociation process proceeded under an isothermal condition. Hereafter, the heat transfer process is ignored in the analysis.

Results of the dissociation experiments and determination of the dissociation rate constant

Snapshots of the dissociation process of a methane hydrate ball are shown in Figure 8. The times in the figure indicate the elapsed time after the dissociation experiment was started by flowing pure water into the cell. The flow rate was $Q = 1.78 \times 10^{-5}$ m^3 s^{-1}, $T = 278.15$ K, and $P = 9.0$ MPa. Note that the appearance of the ball in the horizontal direction was elongated because the shape of the observation cell was cylindrical. Although the pressure and temperature conditions were above the three-phase boundary, the diameter of the methane hydrate ball was found to be reduced over time, arising from dissociation of the methane hydrate. However, no bubble formation was observed around the methane hydrate ball during the dissociation process. Thus, it was confirmed that the dissociation of the methane hydrate occurred as a result of the water flow under the L_w region and that the dissociation would be driven by the molar Gibbs free energy difference between the hydrate phase and the ambient aqueous phase. The appearances of the hydrate ball in

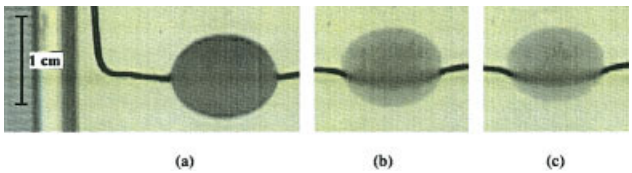

Figure 8. Snapshots of the dissociation process.

MH ball taken at 0 min (a), 10 min (b), and 20 min (c) after the water flow started; $Q = 1.78 \times 10^{-5}$ m^3 s^{-1}, $P = 9.0$ MPa, and $T = 276.15$ K. [Color figure can be viewed in the online issue, which is available at www.interscience.wiley.com.]

Figures 8b and 8c seem slightly transparent. This may be because the hydrate ball is porous and water penetrated into the ball after a certain time. However, it is believed that the dissociation of methane from the interior of the hydrate ball is negligibly small in this study.

The results for the observed overall dissociation rates are shown in Figures 9–11. An example of a calibration curve for C_x vs. k_{bl} is shown in Figure 12 for the conditions of $Q = 1.78 \times 10^{-5}$ m^3 s^{-1}, $P = 9.0$ MPa, and $T = 276.15$ K. The determined values for the dissociation rate constant are shown in Figures 13–15. The upper and lower error ranges are also shown in the figures, by taking into consideration the root-mean-square of the maximum values of possible errors in the CFD calculation and the measurements, such as Sh difference between the CFD and the Rowe–Claxton equation, the accuracies of the flow meter, the manometer, and the thermometer. The dissociation rate constant was almost independent of the pressure and the flow rate, whereas the rate constant increased with increasing temperature. Independence of the flow rate was confirmed within a relatively narrow range of the water flow rate, that is, a single flow range of transitional flow; future testing will be necessary to confirm the universality of the rate constant k_{bl}, covering a wider range of the flow rates, to claim the dissociation rate constant for the present model is intrinsic. For the temperature dependency, an Arrhenius-type equation could be applicable, that is,

$$k_{bl} = A' \exp(-E/RT) \tag{33}$$

where A' is the frequency factor and E is the activation energy. From the plot of k_{bl} vs. $1/T$, the values of $A' = 3.89 \times 10^{12}$ mol^2 J^{-1} s^{-1} m^{-2} and $E = 98.3$ kJ mol^{-1} were obtained. The activation energy is almost the same as that obtained by Clarke and Bishnoi,[7] and in the same order of magnitude as the heat of dissociation ($\approx$54.2 kJ mol^{-1} [25]). This result indicates that the dissociation can occur through an activation process associated with the decomposition of the hydrate lattices.

In Part I of the present study, the dissociation rate constant k_{bl} was determined from the dissociation of methane hydrate induced by the fresh water flow under the conditions where the pressure is above the three-phase boundary for a given temperature. Although the present results are applicable for

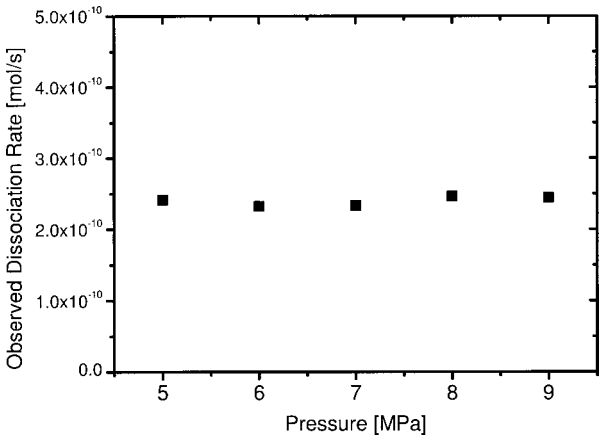

Figure 10. Dependency of the observed overall dissociation of methane hydrate on the pressure.

Volumetric flow rate of the ambient water $Q = 1.78 \times 10^{-5}$ m^3 s^{-1}, $T = 276.15$ K.

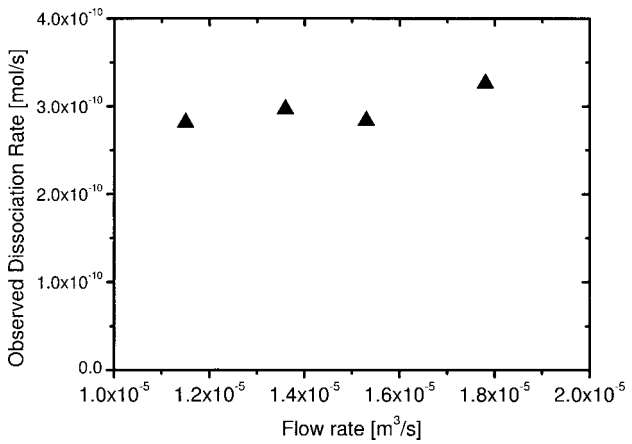

Figure 9. Dependency of the observed overall dissociation of methane hydrate on the volumetric flow rate of the ambient water.

$P = 7.0$ MPa, $T = 280.15$ K.

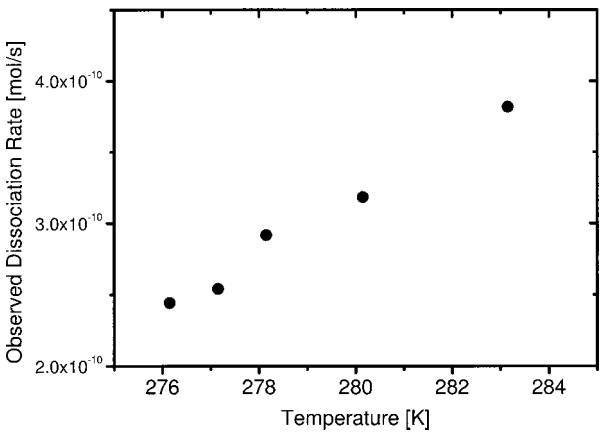

Figure 11. Dependency of the observed overall dissociation of methane hydrate on the temperature.

Volumetric flow rate of the ambient water $Q = 1.78 \times 10^{-5}$ m^3 s^{-1}, $P = 9.0$ MPa.

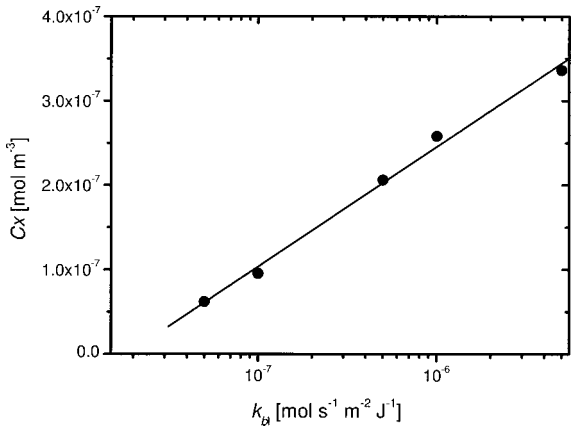

Figure 12. An example of a calibration curve for k_{bl} vs. C_x, assuming the conditions of the volumetric water flow rate $Q = 1.78 \times 10^{-5}$ m^3 s^{-1} and $T = 276.15$ K.

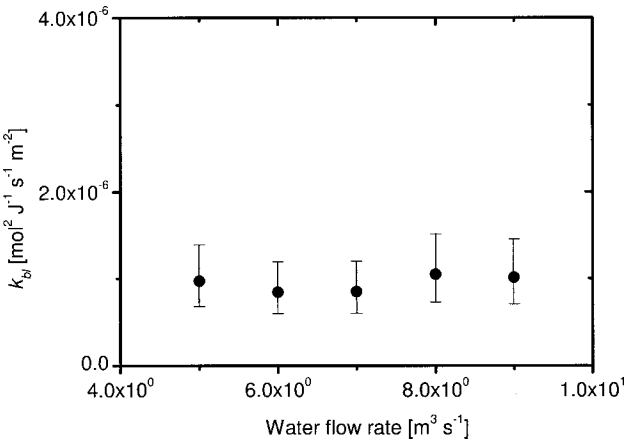

Figure 14. Dependency of the dissociation rate constant of methane hydrate on the pressure.

Volumetric flow rate of the ambient water $Q = 1.67 \times 10^{-5}$ m^3 s^{-1}, $T = 276.15$ K.

the ranges of the conditions used in the study, it can be considered that the present treatment would be extendable for other methods of hydrate dissociation, such as depressurization or temperature increase. The driving force for such cases can also be presumed to be the molar free Gibbs energy difference, which can be converted to the concentration of methane dissolved in the aqueous phase. The same proportionality constant of the dissociation rate to the driving force k_{bl} should be applied irrespective of the dissociation method as far as the driving force is expressed by the molar Gibbs free energy difference. It can be considered that the methodology developed in this study can be extended to other systems such as dissociation process by other driving forces, or for hydrates of other chemical species such as ethane or propane hydrates, which may constitute the natural gas hydrate resources. In Part II of this study, extension of the present treatment to other dissociation methods will be discussed.

Conclusions

Dissociation processes of a methane hydrate ball were observed under conditions above the three-phase (H–L_w–V) boundary where hydrate is thermodynamically stable in terms of the pressure and temperature conditions. Dissociation without the formation of methane bubbles in the aqueous phase was observed, indicating a relatively low dissociation rate in which the concentration of the dissolved methane in the ambient water was kept below the equilibrium solubility. A model describing the dissociation of methane hydrate in contact with the aqueous phase was developed, assuming that the driving force for the dissociation is the molar Gibbs free energy difference between the hydrate phase and the ambient aqueous phase. The dissociation equation was described in terms of the concentration of methane dissolved in water. The rate constant for the dissociation k_{bl} was determined for various conditions of ambient flow rate, pressure, and tem-

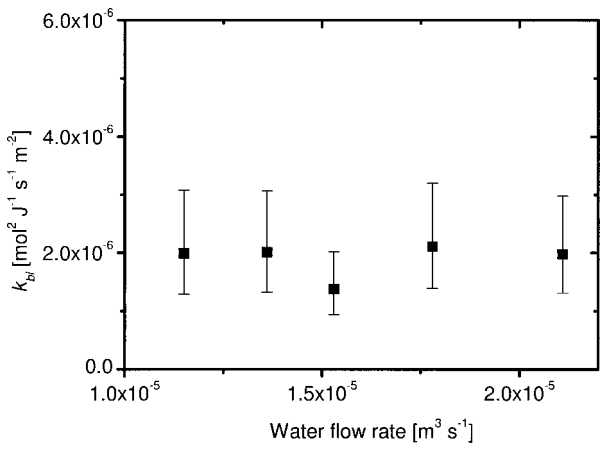

Figure 13. Dependency of the dissociation rate constant of methane hydrate on the volumetric flow rate of the ambient water.

$P = 7.0$ MPa, $T = 280.15$ K.

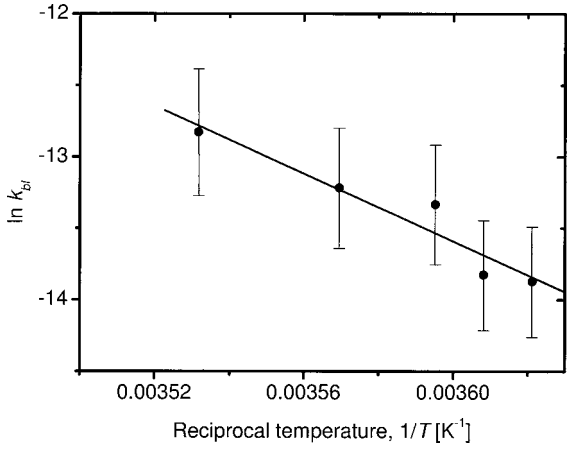

Figure 15. Dependency of the dissociation rate constant of methane hydrate on the temperature.

Volumetric flow rate of the ambient water $Q = 1.78 \times 10^{-5}$ m^3 s^{-1}, $P = 9.0$ MPa.

perature, by combining the experimental results for the overall dissociation and the numerical simulation of the flow by the CFD method. It was shown from the numerical simulation that the surface temperature of the methane hydrate ball was kept equal to that of the ambient water, suggesting that the dissociation process at the surface proceeded under isothermal conditions where the heat transfer process was not the rate-determining step for the dissociation. The obtained value of k_{bl} was independent of the ambient flow rate of water, suggesting that the rate constant is intrinsic within the range studied in this study. It can be expected that the present treatment can be applied to general dissociation processes induced by other types of driving forces as well.

Acknowledgments

This work was financially supported by the MH21 Consortium of Japan. The authors are grateful to Drs. H. Narita and T. Yamaguchi of AIST and Prof. Y. Masuda of University of Tokyo for helpful comments and encouragement.

Notation

A = cross-sectional area of the observation cell, m^2
A' = frequency factor in Eq. 33, $mol^2\ J^{-1}\ s^{-1}\ m^{-2}$
C = volumetric molar concentration of methane in the ambient water, $mol\ m^{-3}$
C' = volumetric molar concentration of methane dissolved in water at the centroid of a cell attaching to the hydrate surface, $mol\ m^{-3}$
C_d = drag coefficient
C_H = volumetric molar concentration of methane in the aqueous solution equilibrated with the stable hydrate phase, $mol\ m^{-3}$
C_I = volumetric molar concentration of methane in the ambient aqueous solution at the surface of the hydrate ball, $mol\ m^{-3}$
C_p = specific heat capacity at constant pressure, $J\ kg^{-1}\ K^{-1}$
C_x = average molar volumetric concentration of methane in the ambient water flow for a given cross section of water flow, $mol\ m^{-3}$
d = diameter of the methane hydrate ball, m
D = diffusion coefficient of methane in water, $m\ s^{-2}$
E = activation energy in Eq. 33, $J\ mol^{-1}$
F = dissociation rate flux, $mol\ s^{-1}\ m^{-2}$
G = molar Gibbs free energy, $J\ mol^{-1}$
ΔG = change of the Gibbs free energy when one mole of the hydrate under a dissociation condition is dissociated into the aqueous phase, $J\ mol^{-1}$
ΔH_{dis} = heat of dissociation per mole hydrate, $J\ mol^{-1}$
h_L = length of the water layer attached on the hydrate surface, m
h_w = hydration number
k_{bl} = dissociation rate coefficient defined in Eq. 4, $mol^2\ J^{-1}\ s^{-1}\ m^{-2}$
k_m = mass transfer coefficient, $m\ s^{-1}$
L = thickness of computational cell, m
P = thermodynamic pressure, Pa
p = fluid-mechanical static pressure, Pa
Q = volumetric flow rate of the ambient water, $m^3\ s^{-1}$
q_H = latent heat of hydrate dissociation, $J\ mol^{-1}$
r_{dis} = rate of hydrate dissociation based on the rate process theory, $mol\ s^{-1}\ m^{-2}$
r_{form} = rate of hydrate formation based on the rate process theory, $mol\ s^{-1}\ m^{-2}$
R = gas constant, 8.314 $J\ K^{-1}\ mol^{-1}$
Re = Reynolds number ($= QdA^{-1}\nu_L^{-1}$)
Sc = Schmidt number ($= {}^{D^{-1}}{}_{L}{}^{-1}$)
Sh = Sherwood number ($= k_m d/D$)
T = absolute temperature, K
T_L = temperatures at the centroids of a cell in the solid hydrate, K
T_H = temperatures at the centroids of a cell in the aqueous phase, K
$\boldsymbol{u}$ = velocity vector of water flow, $m\ s^{-1}$
x = mole fraction of methane
x_{eq} = solubility of methane in the aqueous solution in equilibrium with the stable hydrate phase
x_I = mole fraction of methane in the aqueous phase at the surface of the hydrate ball

Greek letters

α_L = thermal diffusivity ($=\lambda_L\rho_L^{-1}C_{pL}^{-1}$) in the aqueous phase, $m\ s^{-2}$
α_H = thermal diffusivity ($=_{HH}{}^{-1}C_{pH}{}^{-1}$) in the hydrate ball, $m\ s^{-2}$
Δ = thickness of the computational cell, m
δ = thickness of the boundary layer, m
$\Delta\mu$ = chemical potential difference, $J\ mol^{-1}$
λ = heat conductivity, $W\ K^{-1}\ m^{-1}$
μ = chemical potential, $J\ mol^{-1}$
μ_M^* = chemical potential of methane at the reference state, $J\ mol^{-1}$
μ_M^H = chemical potential of methane in the hydrate phase, $J\ mol^{-1}$
μ_M^L = chemical potential of methane in the aqueous phase, $J\ mol^{-1}$
μ_W^H = chemical potential of water in the hydrate phase, $J\ mol^{-1}$
μ_W^L = chemical potential of water in the aqueous phase, $J\ mol^{-1}$
μ_W^0 = chemical potential of water at the reference state, $J\ mol^{-1}$
ν = kinematic viscosity, $m\ s^{-2}$
ρ = density of the ambient water, $kg\ m^{-3}$
ρ_H = density of the hydrate ball, $kg\ m^{-3}$

Subscripts

c = mass concentration
eq = at equilibrium
h = heat
H = hydrate phase
I = interface of methane hydrate and water
L = aqueous phase
m = momentum
M = methane
obs = observed
W = water
WL = water in the aqueous phase
WH = water in the hydrate phase

Superscripts

H = hydrate phase
L = aqueous phase
V = vapor phase

Literature Cited

1. Makogon YF. *Hydrates of Natural Gas*. Tulsa, OK: Penn Well Publishing; 1974.
2. Holder GD, Angert PF. Simulation of gas production from a reservoir containing both gas hydrates and free natural gas. Paper SPE-11105, Proceedings of SPE Conference, New Orleans, LA, Sep. 26–29;1982.
3. Selim MS, Sloan ED. Heat and mass transfer during the dissociation of hydrates in porous media. *AIChE J*. 1989;35:1049–1052.
4. Ullerich JW, Selim MS, Sloan ED. Theory and measurement of hydrate dissociation. *AIChE J*. 1987;33:747–752.
5. Kamath VA, Holder GD. Dissociation heat transfer characteristics of methane hydrates. *AIChE J*. 1987;33:347–350.
6. Kim HC, Bishnoi PR, Heidemann RA, Rizvi SSH. Kinetics of methane hydrate decomposition. *Chem Eng Sci*. 1987;42:1645– 1653.
7. Clarke M, Bishnoi PR. Determination of the activation energy and intrinsic rate constant of methane gas hydrate decomposition. *Can J Chem Eng*. 2001;79:143–147.
8. Sean W-Y, Sato T, Yamasaki A, Kiyono F. Development of dissociation model of methane hydrate based on numerical and physical experiments. *Proceedings of the Fifth International Conference on Gas Hydrates;* 2005;1:104–112.
9. Kashchiev D, Firoozabadi A. Driving force for crystallization of gas hydrates. *J Crystal Growth.* 2002;241:220–230.
10. de Groot SR, Mazur P.*Non-Equilibrium Thermodynamics*. New York: Dover; 1984.
11. Wood SE, Battino R.*Thermodynamics of Chemical Systems*. Cambridge, UK: Cambridge Univ. Press; 1990.
12. Seo Y, Lee H, Ryu BJ. Hydration number and two-phase equilibria of CH_4 hydrate in the deep ocean sediments. *Geophys Res Lett*. 2002;29:85–1–85–4.

13. Kuustraa VA, Hammershaimb EC.*Handbook of Gas Hydrate Properties and Occurrence*. Charleston, WV: Lewin & Associates; 1983.
14. Chemical Society of Japan. *Kagaku Binran* (Handbook for Chemists). Tokyo: Maruzen; 1985 (in Japanese).
15. Masuda Y, Fujinaga Y, Naganawa S, Fujita K. Modeling and experimental studies on dissociation of methane gas hydrates in Berea sandstone cores. Proceedings of the 3rd International Conference on Gas Hydrates, Salt Lake City, UT, July 18–22; 1999.
16. Jung R-T, Sato T. Numerical simulation of high Schmidt number flow over a droplet by using moving unstructured mesh. *J Comput Phys*. 2005;203:221–249.
17. Rhie CM, Chow WL. Numerical study of the turbulent flow past an airfoil with training edge separation. *AIAA J*. 1983;21:1525–1532.
18. Rowe PN, Claxton KT. Heat and mass transfer from a single sphere in an extensive flowing fluid. *Trans IChemE*. 1965;43:14–31.
19. Whitaker S. Forced convection heat transfer correlations for flow in pipes, past flat plates, single cylinders, single spheres, and for flow in packed beds and tube bundles. *AIChE J*. 1972;18:361–371.
20. Ranz W, Marshall W. Evaporation from drops: Part I. *Chem Eng Prog*. 1952;48:141–146.
21. Lapple CE. *Particle Dynamics*. Wilmington, DE: E.I. DuPont de Nemours and Co.; 1951.
22. Clift R, Grace JR, Weber ME. *Bubbles, Drops, and Particles*. New York: Academic Press; 1978:380.
23. Handa YP. Compositions, enthalpies of dissociation, and heat capacities in the range 85 to 270 K for clathrate hydrates of methane, ethane, and propane, and enthalpy of dissociation of isobutane hydrate, as determined by a heat-flow calorimeter. *J Chem Thermodyn*. 1986;18:915–921.
24. Kawamura T, Komai T, Yamamoto Y, Nagashima K, Ohga K, Higuchi K. Growth kinetics of CO_2 hydrate just below melting point of ice. *J Crystal Growth*. 2002;234:220–226.
25. Sloan ED.*Clathrate Hydrates of Natural Gases*. New York: Marcel Dekker; 1988.

Manuscript received July 21, 2006, and revision received Oct. 12, 2006.